A Linear Spectral Model of Tropical Mesoscale Systems: Sensitivity Studies

MARIA F. SILVA DIAS[1]

National Center for Atmospheric Research,[2] Boulder, CO 80307

ALAN K. BETTS

West Pawlet, VT 05775

DUANE E. STEVENS

Department of Atmospheric Science, Colorado State University, Fort Collins, CO 80523

(Manuscript received 10 August 1983, in final form 14 February 1984)

ABSTRACT

A revised version of Raymond's wave-CISK model is used to study the propagation of mesoscale modes. The sensitivity of unstable modes to variations in basic state stability and wind shear (characteristics of the eastern Atlantic during GATE), as well as parameterized cumulus heating, is examined. Unstable modes exist for mesoscale wavelengths, which are sensitive to the details of the cumulus heating parameters as well as the structure of the large-scale wind shear. In many cases, the most unstable mode has a two-dimensional structure.

1. Introduction

Previous attempts to model mesoscale motion fall into two main categories: modeling of the cumulonimbus scale with horizontal dimensions up to 30 km and modeling of a larger scale with dimensions up to 100 km. The essential difference between these two areas is the inclusion, through parameterization schemes, of different physical processes. The models of the cumulonimbus scale are nonhydrostatic and close the system of governing equations by parameterizing microphysical and sometimes turbulent processes. The results are extrapolated to explain features of convective lines on the mesoscale, such as the role of organized mesoscale updrafts and downdrafts. In this type of model we may include those by Moncrieff and Miller (1976), Klemp and Wilhelmson (1978a,b) and Cotton and Tripoli (1978). A common denominator among these models is the fact that they lead to the conclusion that the environmental wind shear is extremely important in determining the properties of small-scale systems, particularly their propagation.

Models of the larger mesoscale are usually hydrostatic and some use sophisticated parameterization schemes to represent cumulus-scale moist processes. Typical parameters and processes include cloud base, cloud top, updraft and downdraft thermodynamics, entrainment and detrainment effects, precipitation, condensation and evaporation. The Kreitzberg and Perkey (1976, 1977) and Fritsch (1978) models take into account cloud lifetimes as opposed to Brown's (1979) model that makes the quasi-equilibrium assumption (Arakawa and Schubert, 1974). Brown's model shows results that bear strong resemblance to observed mesoscale systems; however, because of the relatively complicated physical parameterizations, these models do not illuminate well the fundamental dynamical processes.

Some simpler models have been proposed. Raymond (1975, 1976), presents a linear model using a parameterization scheme based on low-level convergence, following the wave-CISK concept (Lindzen, 1974), to study the dynamic structure on the mesoscale at early stages of development. Fernandez and Thorpe (1979) have recently made a comparison between the steady state models of Moncrieff and Green (1972) and Moncrieff and Miller (1976) and the wave-CISK model of Raymond (1975, 1976). They conclude that Raymond's model gives poor results when cloud bases are very low, indicating that the mass flux due to the plumes should be treated in a more realistic way. They also conclude that the ability of storms to propagate relative to the environmental flow can be reproduced in the linear wave-CISK model and thus may not be a fundamentally nonlinear effect.

[1] On leave from Instituto Astronômico e Geofísico, Universidade de São Paulo, Brazil.

[2] The National Center for Atmospheric Research is sponsored by the National Science Foundation.

This paper presents an extension of Raymond's (1975, 1976) wave-CISK model using the heating parameterization of Stevens and Lindzen (1978). The sensitivity of the unstable modes to the parameterization schemes and to environmental conditions such as wind shear are presented. Unstable modes are found to exist for mesoscale wavelengths (~20 km), but there is considerable sensitivity to cumulus heating parameters and the structure of the large-scale flows. As there is not general concensus on the existence or uniqueness of a cumulus parameterization scheme for meso- and larger scales, the sensitivity to parameters is distressing.

The finding of greatest instability at an intermediate scale is a new result which depends on the wind shear in a wave-CISK model. Essentially two-dimensional instabilities, with one horizontal scale much larger than the other, are encouragingly reminiscent of squall line activity in the tropics. A weakness of this and other wave-CISK studies is the lack of a clear separation of scales between cumulus and mesoscale. Nevertheless, the intermediate scale selection suggests progress beyond conditional instability of the first kind (i.e., at infinitesimal scale in a model without dissipation).

2. Governing equations

The governing equations are the conservation of momentum, thermodynamic energy and mass:

$$\frac{\partial \mathbf{v}}{\partial t} + \mathbf{v}\cdot\nabla\mathbf{v} + f\hat{\mathbf{k}}\times\mathbf{v} + \frac{1}{\rho}\nabla p + g\hat{\mathbf{k}} = 0, \quad (1)$$

$$\frac{\partial \theta}{\partial t} + \mathbf{v}\cdot\nabla\theta = Q, \quad (2)$$

$$\frac{\partial \rho}{\partial t} + \nabla\cdot(\rho\mathbf{v}) = 0. \quad (3)$$

The symbols have the usual meanings; $\hat{\mathbf{k}}$ is the vertical unit vector.

Several assumptions are made concerning the above set of equations:

(i) Separation of scales is assumed between the horizontally averaged basic state or large-scale (subscript zero) and deviations from it (primed variables) which contain mesoscale and small-scale contributions. The basic state variables are required to satisfy (1)–(3), as does the *sum* of the basic state and deviation quantities represented by the nonsubscripted, nonprimed variables. Subtraction of the former set of equations from the latter provides a set of equations for the primed variables.

(ii) The model is formulated for a nonrotating plane ($f = 0$). The neglect of the earth's rotation in a mesoscale model may be considered a valid first approximation, especially in the tropical regions where the local Coriolis parameter is much smaller than the Doppler-shifted frequency and therefore the Rossby number exceeds unity.

(iii) The anelastic form of the continuity equation is assumed. The linearized version of Poisson's equation is used to eliminate the dependence on perturbation density. To be consistent with the anelastic assumption, we neglect in the vertical component of the momentum equation a term

$$\frac{p'}{\rho_0}\frac{d\ln\theta_0}{dz}$$

(Charney and Eliassen, 1964). Scale analysis shows that this term is one order of magnitude smaller than $g\theta'/\theta_0$.

The above assumptions lead to the system of perturbation equations

$$\frac{\partial \mathbf{v}'}{\partial t} + \mathbf{v}_0\cdot\nabla\mathbf{v}' + \mathbf{v}'\cdot\nabla\mathbf{v}_0 + \nabla\frac{p'}{\rho_0} - \frac{\theta'}{\theta_0}g\hat{\mathbf{k}} = \psi, \quad (4)$$

$$\frac{\partial \theta'}{\partial t} + \mathbf{v}_0\cdot\nabla\theta' + \mathbf{v}'\cdot\nabla\theta_0 = Q' + \psi_\theta, \quad (5)$$

$$\nabla\cdot(\rho_0\mathbf{v}') = 0, \quad (6)$$

where

$$-\psi = \left(\mathbf{v}'\cdot\nabla\mathbf{v}' + \frac{\rho'}{\rho_0^2}\nabla p'\right), \quad -\psi_\theta = (\mathbf{v}'\cdot\nabla\theta'). \quad (7)$$

A further step is taken now to separate the primed variables into mesoscale and small-scale contributions. Mathematically, this separation of scales requires a simple averaging technique. Physically, however, there is no certainty that this is possible or even reasonable since very little is known about scale interaction from the observational point of view. A justification for the widespread use of this technique is that different physical mechanisms govern the motions in each scale: for example, microscale turbulence may play a minor role in long atmospheric waves and mesoscale motions, but significantly affects cumulus-scale phenomena. On the assumption that the two mentioned scales may be separated, a running average is defined

$$\langle\mathbf{v}'(x, y, z, t)\rangle = \frac{1}{\Delta x\Delta y}\int_{x-\Delta x/2}^{x+\Delta x/2}\int_{y-\Delta y/2}^{y+\Delta y/2}\mathbf{v}'(x', y', z, t)dx'dy', \quad (8)$$

so that the perturbation fields may be written as

$$\mathbf{v}' = \langle\mathbf{v}'\rangle + \mathbf{v}'', \quad (9)$$

where the double prime refers to the residual after the running average is performed and corresponds to the small-scale contribution. The angular brackets correspond to the mesoscale contribution. We shall use Δx, $\Delta y \approx 10$ km which should be adequate to resolve mesoscale motions.

The system of equations (4)–(7) undergo the following transformations:

(i) The running average is performed;
(ii) the system is linearized through neglect of correlations between mesoscale variables. Small-scale transports are retained.

With the choice of a horizontally homogeneous basic state, we now decompose mesoscale variables into their Fourier components [assuming for the moment a single-valued complex frequency $\omega(\mathbf{k})$]:

$$\langle v'(x, y, z, t)\rangle = \int_{-\infty}^{+\infty}\int \hat{v}(\mathbf{k}, z)\exp[i(\mathbf{k}\cdot\mathbf{r} - \omega t)]dk_x dk_y, \tag{10}$$

where

$$\mathbf{k} = k_x\hat{\mathbf{i}} + k_y\hat{\mathbf{j}}, \quad \mathbf{r} = x\hat{\mathbf{i}} + y\hat{\mathbf{j}}. \tag{11}$$

The above assumptions reduce the problem to solving the following equations

$$-i(\omega - \mathbf{k}\cdot\mathbf{v}_0)\hat{u} + \frac{du_0}{dz}\hat{w} + i\frac{k_x}{\rho_0}\hat{p} = \hat{\psi}_x, \tag{12}$$

$$-i(\omega - \mathbf{k}\cdot\mathbf{v}_0)\hat{v} + \frac{dv_0}{dz}\hat{w} + i\frac{k_y}{\rho_0}\hat{p} = \hat{\psi}_y, \tag{13}$$

$$-i(\omega - \mathbf{k}\cdot\mathbf{v}_0)\hat{w} + \frac{d}{dz}\frac{\hat{p}}{\rho_0} - g\frac{\hat{\theta}}{\theta_0} = \hat{\psi}_z, \tag{14}$$

$$-i(\omega - \mathbf{k}\cdot\mathbf{v}_0)\hat{\theta} + \frac{d\theta_0}{dz}\hat{w} = \hat{Q} + \hat{\psi}_\theta, \tag{15}$$

$$i\mathbf{k}\cdot\hat{\mathbf{v}} + \frac{1}{\rho_0}\frac{d}{dz}(\rho_0\hat{w}) = 0. \tag{16}$$

The problem is then to 1) define a basic state, 2) choose parameterization schemes that will account for the right-hand side of Eqs. (12)–(15), 3) impose boundary conditions and 4) solve the resulting linear, homogeneous system as an eigenvalue problem. For each vector wavenumber $\mathbf{k}$ there is a set of complex frequencies $\omega = \omega_r + i\omega_i$ that satisfy Eqs. (12)–(16). From Eq. (10) it may be seen that positive ω_r corresponds to propagation in the direction of the wavenumber vector $\mathbf{k}$ and negative ω_r to propagation in the opposite direction. Positive ω_i corresponds to exponential growth of the particular mode under consideration and negative ω_i corresponds to exponential decay.

To solve Eqs. (12)–(16), a vertical differencing scheme has to be devised since vertical derivatives are not analytical and large-scale fields depend on height. Following the scheme proposed by Arakawa and Lamb (1977), the atmosphere has been divided into N layers separated by $N - 1$ levels of constant z. The layers carry the horizontal components of velocity $\hat{u}$ and $\hat{v}$, potential temperature $\hat{\theta}$ and pressure $\hat{p}$. The levels carry the vertical velocity $\hat{w}$. Fig. 1 shows the vertical structure of the model.

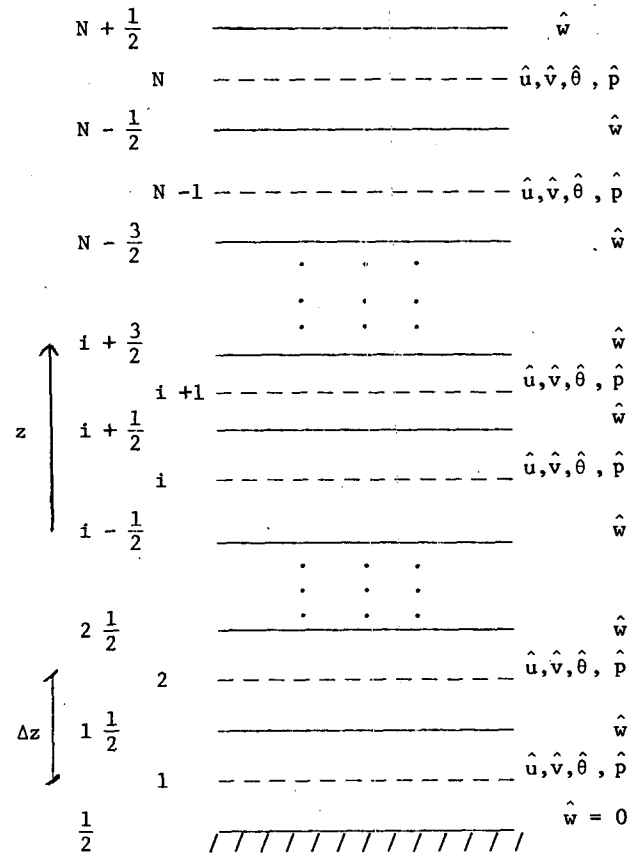

FIG. 1. Model vertical structure showing distribution of variables. Solid lines indicate the levels dividing the layers; dashed lines indicate layers within which the indicated variables are carried.

The boundary condition at the (flat) surface is that the vertical velocity vanishes. At the top of the model, the radiation condition is applied following the procedure used by Eliassen and Palm (1960): it consists of imposing, as the solution in the uppermost layer, an expression for the vertical velocity that allows tropospheric energy to be radiated away to upper levels. Eliassen and Palm (1960), Charney and Pedlosky (1963) and Lindzen (1974) discuss the choice of an upper boundary condition which corresponds to upward energy flux. In the present case, the upper boundary condition is

$$\frac{1}{k}(\omega - \mathbf{v}_0\cdot\mathbf{k})\frac{d}{dz}(\rho_0^{1/2}\hat{w}) + i\left(g\frac{d\ln\theta_0}{dz}\right)^{1/2}(\rho_0^{1/2}\hat{w}) = 0. \tag{17}$$

In this form, a uniform basic state wind is assumed above the top model layer and a term

$$\frac{1}{k^2}\left(\mathbf{k}\cdot\mathbf{k} + \frac{1}{4H^2}\right)(\omega - \mathbf{v}_0\cdot\mathbf{k})^2,$$

which appears as a subtraction to $gd\ln\theta_0/dz$, has been neglected because 1) it is two orders of magnitude smaller than $gd\ln\theta_0/dz$ and 2) it would make the so-

lution of the eigenvalue problem more complicated (i.e., nonlinear in ω).

After the vertical discretization scheme has been applied and the boundary conditions imposed, the system (12)–(16) forms a linear homogeneous system of equations provided the parameterization schemes of heating and eddy momentum transports are a linear function of the dependent variables. In this case, the discretized system may be written as

$$(\mathbf{A} - \omega\mathbf{B})\hat{\mathbf{Z}} = 0, \tag{18}$$

where

$$\hat{\mathbf{Z}} = (\hat{u}_1, \hat{v}_1, \hat{p}_1, \hat{\theta}_1, \hat{w}_{1\text{-}1/2}, \hat{u}_2, \hat{v}_2, \cdots \cdots, \hat{u}_{N-1}, \hat{v}_{N-1}, \hat{p}_{N-1}, \hat{\theta}_{N-1}, \hat{w}_{N-1/2}, \hat{u}_N, \hat{v}_N, \hat{p}_N, \hat{\theta}_N, \hat{w}_{N+1/2}), \tag{19}$$

and $\mathbf{A}$ and $\mathbf{B}$ are $5N \times 5N$ matrices of the coefficients defined by Eqs. (12)–(16). Eq. (18) is the representation of a complex generalized eigenvalue problem, where the frequency ω is the eigenvalue and $\hat{\mathbf{Z}}$ is the corresponding eigenvector. This representation has been used by Yamasaki (1969). However, there are only $3N$ independent eigenvectors because it is possible to eliminate $\hat{u}$, $\hat{p}$ from (12), (13), (14) and (16) to give only $3N$ prognostic equations.

Pedlosky (1964) and Koss (1976) have discussed the representation of initial conditions using a discrete set of eigensolutions.

Raymond (1976) defined the initial condition at the surface only and let the vertical structure be determined by the eigenfunctions of interest, namely, one corresponding to the most unstable mode. The surface initial condition may then be reproduced if enough wavenumbers are considered. The procedure to be followed here will be a generalization of Raymond's approach.

We use all $3N$ modes which may be unstable, neutral or stable. To allow an arbitrary initial condition to be represented, Eq. (10) may be written for all variables in vector form as

$$\mathbf{Z}(x, y, t) = \mathbf{Z}_0 + \int_{-\infty}^{\infty}\int \tilde{\mathbf{Z}}(\mathbf{k}, t)e^{i\mathbf{k}\cdot\mathbf{r}}dk_x dk_y, \tag{20}$$

where

$$\mathbf{Z}(x, y, t) = [u_1(x, y, t), v_1(x, y, t), p_1(x, y, t), \theta_1(x, y, t), w_{1\text{-}1/2}(x, y, t), u_2(x, y, t), \ldots, u_N(x, y, t), v_N(x, y, t), p_N(x, y, t), \theta_N(x, y, t), w_{N+1/2}(x, y, t)], \tag{21}$$

and $\mathbf{Z}_0$ contains the given basic state variables. At $t = 0$, the Fourier transform of Eq. (20) gives

$$\tilde{\mathbf{Z}}(\mathbf{k}, 0) = \frac{1}{(2\pi)^2}\int_{-\infty}^{+\infty}\int [\mathbf{Z}(x, y, 0) - \mathbf{Z}_0]e^{-i\mathbf{k}\cdot\mathbf{r}}dxdy. \tag{22}$$

We define

$$\tilde{\mathbf{Z}}(\mathbf{k}, t) = \sum_{m=1}^{3N} C(\mathbf{k}, m)\hat{\mathbf{Z}}(\mathbf{k}, m)e^{-i\omega(\mathbf{k},m)t}, \tag{23}$$

where the summation is over all the modes (unstable, stable and neutral) which are eigensolutions of (18) for each $\mathbf{k}$. The coefficient $C(\mathbf{k}, m)$ may be determined at $t = 0$ by using the $3N$ variables in $\tilde{\mathbf{Z}}(\mathbf{k}, 0)$ which correspond to the set of linearly independent solutions.

Given the initial condition and its Fourier transform through (22), Eq. (23) may be solved as a linear system of $3N$ equations in $3N$ unknowns.

Evaluation of the integrals in (20) and (22) requires discretization in which the integrals are replaced by sums. With discretization of the Fourier transforms and subsequent truncation of the series, the boundedness conditions at an infinite horizontal distance are replaced by periodicity at the largest scale resolved. In the present case, $\mathbf{k} = n_x(2\pi/L_x\hat{i}) + n_y(2\pi/L_y\hat{j})$, with $L_x = L_y = 300$ km and n_x, n_y ranging from -30 to $+30$. For $n_x = n_y = 30$ the wavelength is 7.1 km.

In this paper, the sensitivity of ω to different parameters and to environmental conditions is tested; the evolution of an initial condition will be presented in a later paper.

3. Parameterization of small-scale processes

The model described in this paper is intended for mesoscale analysis and, with this purpose, will look into scales from ten to a few hundred kilometers. The cumulus scale falls into the smaller scale and obviously plays a very important role in the description and understanding of mesoscale motions; therefore, we parameterize the cumulus scale. This is a crucial step, however, since relatively little is known of the detailed interaction between cumulus-scale and mesoscale motions.

a. Cumulus heating

The diabatic heating in the cumulus scale affects the mesoscale temperature fields through the term $\hat{\psi}_\theta$ on the right-hand side of Eq. (15). The horizontal advection of temperature by the small scale in $\hat{\psi}_\theta$ will be neglected under the assumption that the adiabatic heating rate offers a bigger contribution. A future revision of this model might attempt to include these terms perhaps through the so-called pseudo-viscosity concept used to parameterize turbulent transports (see Cotton, 1975). Here $\hat{Q}$ is the mesoscale diabatic heating and is neglected since there is no mesoscale moisture field in the present model. All the moisture is in the cumulus-scale processes.

The CISK (Conditional Instability of the Second Kind) mechanism, as envisioned by Ooyama (1963), Charney and Eliassen (1964) and very well described by Ooyama (1969), is based on the idea that cumulus

clouds and large-scale tropical systems support each other, the cumulus cells by supplying the heat energy for driving the depression and the depression by providing low-level convergence of moisture into the cumulus cells.

This physical mechanism may be used to explain interaction between the cumulus scale and the mesoscale as well, even if the time scale of mesoscale events is not as long as that of large-scale systems, because the convergence supplied by mesoscale systems is typically one or two orders of magnitude larger than that provided by large-scale systems.

We define the heating function

$$\hat{\psi}_\theta = \eta(z)\hat{w}_{ML}, \tag{24}$$

where $\hat{w}_{ML}$ is the vertical velocity at the top of the moist layer (z_{ML}) and $\eta(z)$ is specified by the profile

$$\eta(z) = \begin{cases} \alpha\left(\dfrac{p_{00}}{p}\right)^{\kappa} \exp(bz) \sin\left(\pi \dfrac{z - z_C}{z_T - z_C}\right), \\ \qquad\qquad z_C \leqslant z \leqslant z_T \\ 0, \quad z \leqslant z_C \text{ or } z \geqslant z_T, \end{cases} \tag{25}$$

where z_C and z_T are cloud base and cloud top respectively and b is adjusted to change the level of maximum heating rate (z_{MH}).

Stevens and Lindzen (1978) constrained α, the intensity of the heating rate using a precipitation budget. We shall instead impose the constraint

$$\eta(z_{ML}) = \delta \frac{d\theta_0}{dz}(z_{ML}). \tag{26}$$

For $\delta = 1$, this condition ensures that the parameterized cumulus heating equals the mesoscale adiabatic cooling at the level z_{ML}. Sensitivity to δ is shown in Table 1. Emanuel (1982) recommends that δ remain less than or equal to 1, otherwise, conditional instability of the first kind will result.

b. *Momentum mixing*

Observational studies (e.g., Houze, 1973) have shown that vertical momentum transport by cumulus may be of the same order of magnitude as the large-scale vertical momentum transport. The mesoscale contribution and cumulus-scale contribution are diagnosed as a single quantity so that no real assessment of the former has been done. In modeling the mesoscale motions, the cumulus-scale transports also play an important role. Schneider and Lindzen (1976) parameterized the momentum exchange by cumulus convection for use in large-scale models of the tropical atmosphere. Experiments using this parameterization in this mesoscale model are in progress. In this paper, we present only results in which momentum transport by the small-scale are neglected (i.e., for which $\psi_x = \psi_y = \psi_z = 0$) and the mesoscale transports are explicitly computed.

4. Model vertical structure

The model vertical structure may be seen in Fig. 1. The top boundary is placed just above the tropopause at 16 km. The model vertical resolution was set at 1 km so that there are 16 levels in the vertical. Tests using vertical spacing less than 1 km showed that the eigenvalues were essentially unmodified. However, decreasing the resolution to 2 km from 1 km produced eigenvalues that differ by as much as 50%. The model without any parameterization scheme is able to reproduce the speed of internal gravity waves and instability characteristics of waves produced by shear instability in stratified flows (Silva Dias, 1979).

5. Sensitivity to small-scale parameterizations

The basic state is derived from the mean state during GATE as computed by Thompson *et al.* (1979). Fig. 2 shows the wind hodograph labeled East Atlantic (hereafter E Atlantic) which was obtained by averaging the winds in the B-scale during GATE. It may be noted that there is considerable directional shear of the winds from the surface up to 700 mb. Above that level, the winds are basically from the east. Fig. 3 shows the

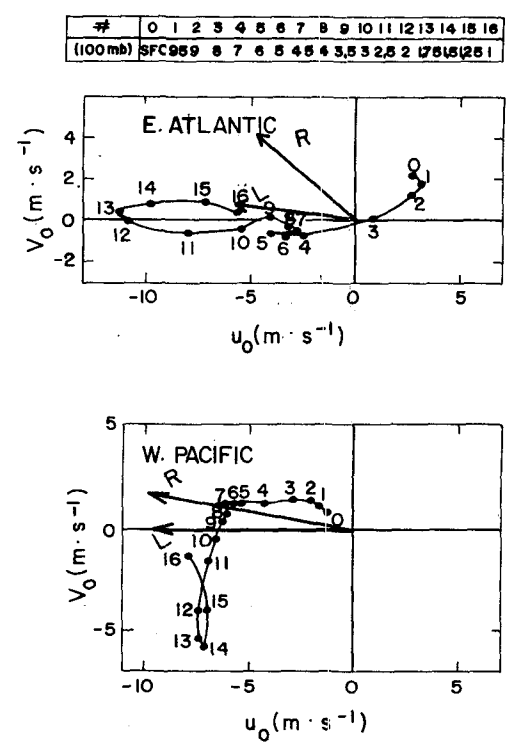

FIG. 2. Wind hodographs for GATE B-scale (E Atlantic) from Thompson *et al.* (1979) and for KEP triangle (W Pacific) from Reed and Recker (1971). L, R denote group velocity vectors associated with left- and right-moving modes.

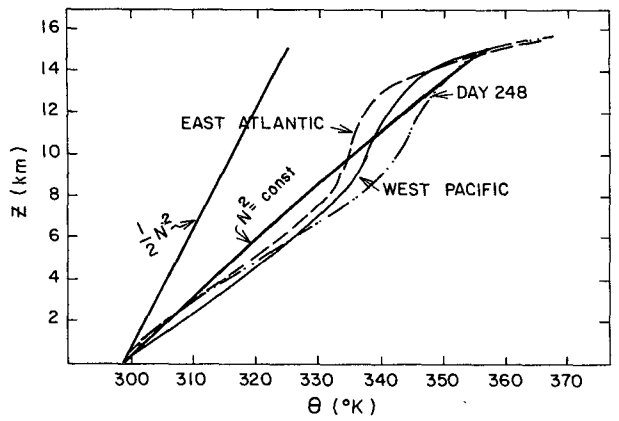

FIG. 3. Potential temperature for GATE B-scale (E Atlantic) from Thompson *et al.*, (1979), for KEP triangle (W Pacific) from Reed and Recker (1971) and for the mean between temperature soundings in the ships *Dallas* and *Oceanographer* on 5 September 1974 at 900 GMT (Day 248) during GATE. Also shown are the constant static stability profiles used in sensitivity tests.

potential temperatures labeled E Atlantic for the same period. In this section, we shall use a simplification of profiles in Figs. 2 and 3: the east–west component of the E Atlantic profile and a constant static stability profile.

a. *Cumulus heating parameters*

Table 1 shows the range of variation allowed for each of the cumulus heating parameters. Cloud base height z_C has been varied between 0.5 and 1.5 km. Cloud top height has been varied between 10 and 14 km. Observations during GATE report cloud bases between 400 and 600 m and tops of cumulonimbus from 10 to 15 km (Houze and Cheng, 1977).

The height of the top of the moist layer z_{ML} has been allowed to vary between 1 and 3 km. It is assumed that most of the moisture convergence in a column occurs in the moist layer; according to Gray (1977) the strongest convergence in GATE systems occurs below about 800 mb or 2 km.

The level of maximum heating rate z_{MH} has been varied from 4.5 to 9 km. Nitta (1977), in a large-scale budget of periods with different levels of mesoscale activity, found the level of maximum heating rate to be at 7.5 km. Yanai *et al.* (1973) also found z_{MH} at 7.5 km. Thompson *et al.* (1979) found the level of maximum heating rate at 4.5 km. Williams and Gray (1973) report this level at about 8.5 km. Johnson (1978) reports z_{MH} between 6 and 8 km. It is not known if the variability of z_{MH} in diagnostic studies is due to mesoscale or convective-scale differences, or to the pronounced life cycle changes observed in convective systems (Betts, 1978).

b. *Eigenvalues*

The eigenvalue computation has been run for different wavenumbers (n_x, n_y) for case 1 (Table 1). The solution of (18) produces a set of eigenvalues, the most unstable one being the one with greatest imaginary

TABLE 1. Sensitivity of scale selection, phase velocity and group velocity with regard to cumulus heating parameters.

Case	z_C (km)	z_T (km)	z_{ML} (km)	z_{MH} (km)	Heating intensity parameter δ	Growth rate (10^{-5} s^{-1})	Scale selection (n_x, n_y)	Phase velocity (m s^{-1})	Group velocity (m s^{-1})	Direction from (deg)
1	0.5	12	2	7.5	1	305	(±14, 0)	±6.6	7.6	90
2	1.5	12	2	7.5	1	934	(±16, 0)	±3.6	5.0	90
					1	922	(0, 16)	0.	3.9	90
3	0.5	10	2	7.5	1	625	(±12, 2)	±3.2	5.0	86 94
					1	612	(0, 12)	0.	3.6	93
4	0.5	14	2	7.5	1	228	(±14, 0)	±6.9	5.8	90
5	0.5	12	1	7.5	1	792	(±8, 12)	±2.5	4.7	78 102
					1	736	(±16, 0)	±4.0	4.6	90
6	0.5	12	3	7.5	1	209	(±12, 0)	±6.0	4.8	270
7	0.5	12	2	4.5	1	—	*			
8	0.5	12	2	6.0	1	184	(±16, 0)	±6.2	4.7	90
9	0.5	12	2	9.0	1	702	(±12, 0)	±2.4	4.0	90
10	0.5	12	2	7.5	0.5	—	*			
11	0.5	12	2	7.5	1.5	866	(±8, 16)	±1.1	3.0	73 107

* No scale selection.

part ω_i or fastest growth rate. Fig. 4 shows the most unstable eigenvalues for $n_x = -30, \ldots, 0, \ldots, 30$ and $n_y = 0, \ldots, 30$. The part of the diagram corresponding to $n_y = -30, \ldots, 0$ is not shown because it is equivalent to that shown (by point symmetry through the origin). It is easily verified from (12)–(16) that if ω is a solution for wavenumber (n_x, n_y), then $-\omega^*$ (* denoting complex conjugate) is a solution for wavenumber $(-n_x, -n_y)$, so that the real part of ω changes sign and the imaginary part corresponds to an unstable mode. Figs. 4a, b show isopleths of ω_r and ω_i, respectively, for the most unstable mode. In Fig. 4b it may be noted that the growth rate attains a maximum value for a single mode which is represented by wavenumbers (−14, 0) and (14, 0), i.e., for about 20 km wavelength scale in the east–west direction and infinite wavelength in the north–south direction.

The growth rate of this mode, expressed in terms of $1/\omega_i$, is 5.5 min. Raymond (1975) obtained growth rates of the same order of magnitude for similar wavelengths. This mode travels toward the west with phase speed of 6.6 m s^{-1}. In Fig. 4a, the upper right and left corners show a reversal of the sign of phase speed due to the fact that a different mode has become the most unstable mode.

The scale selection seen in Fig. 4b has not been obtained with wave-CISK type models (Hayashi, 1970; Lindzen, 1974) which do not include basic state wind shear. Raymond (1975) and Sun (1978) also found scale selection similar to the one obtained here.

c. *Group velocity*

The group velocity is defined in neutral wave studies as the velocity at which a packet of waves with slightly different wavelengths will propagate; this is given by (see Bretherton, 1969)

$$\mathbf{C}_g(k_x, k_y) = \frac{\partial \omega_r}{\partial k_x}\mathbf{i} + \frac{\partial \omega_r}{\partial k_y}\mathbf{j}.$$

In the case of a non-neutral packet of waves, the expression above is valid at the initial stage of growth, although as a particular wave with higher growth rate starts to predominate, the propagation velocity will tend to the *phase speed* of this particular unstable mode.

d. *Sensitivity to cumulus heating parameters*

Table 1 summarizes the results of varying z_C, z_T, z_{ML}, z_{MH} and the heating intensity δ in terms of wave-

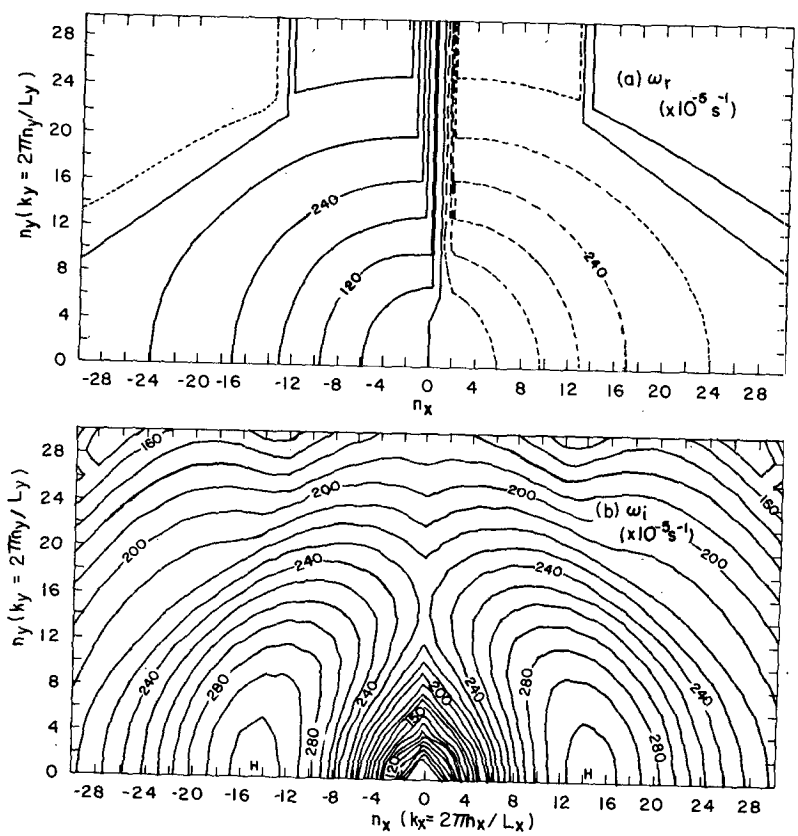

FIG. 4. Eigenvalues of Eq. (18) corresponding to conditions of case 1 of Table 1. (a) ω_r (b) ω_i.

number of maximum growth rate, phase velocity and group velocity derived from diagrams similar to Fig. 4. In a few cases where there was another local maximum in growth rate, of comparable magnitude, it has been listed in order of decreasing growth rate.

There is some variability in the resulting wavenumber of scale selection, phase velocity and group velocity.

The least sensitive result seems to be the wavenumber of maximum growth rate. Except in the last case where there is excessive cumulus heating, if there is scale selection, one of the modes selected is for wavenumbers $(14 \pm 2, 0 \pm 2)$. However, for case 7 where the level of maximum heating rate is low (at 4.5 km) and case 10 where the heating intensity is less than the mesoscale adiabatic cooling–heating term, there is no selection of most unstable mode: growth rates keep increasing toward lower wavelengths as in classical wave-CISK type instability computations.

Phase velocity appears sensitive to cloud base (z_C) and cloud top (z_T) as well as the height of the moist layer z_{ML} and the level of maximum heating z_{MH}.

The effect of changing the top of the moist layer (z_{ML}) is not straightforward and is very much model-dependent due to the particular vertical stratification and vertical extent of the model. When the top of the moist layer is changed, the vertical velocity that is used in the cumulus heating parameterization is also changed [cf. Eqs. (24) and (26)].

The effect of changing the heating amplitude has been discussed by Chang (1976). His model, however, did not include vertical shear of basic state wind. He showed that the growth rate increased approximately linearly with increasing heating while the phase speed remained constant. With wind shear, we find the same conclusion regarding the growth rate, but the phase speed is sensitive to the cumulus heating intensity.

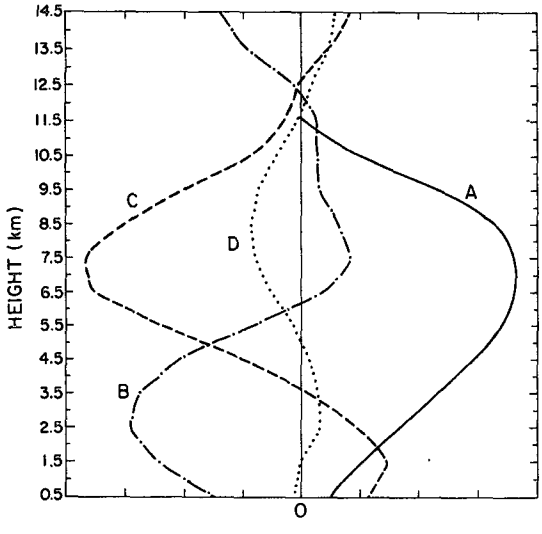

FIG. 5. Vertical structure of terms in the thermodynamic equation (15) for most unstable mode at wavenumber (−24, 20). See text for details; $c_r = -10.8$ m s^{-1}, e-folding growth time = 405 s. A (solid line): $-\eta(z)w_{ML}$; B (dot-dash line): $wd\theta_0/dz$; C (dashed line): $d\theta/dt$; D (dotted line): $\mathbf{v}\cdot\nabla\theta$.

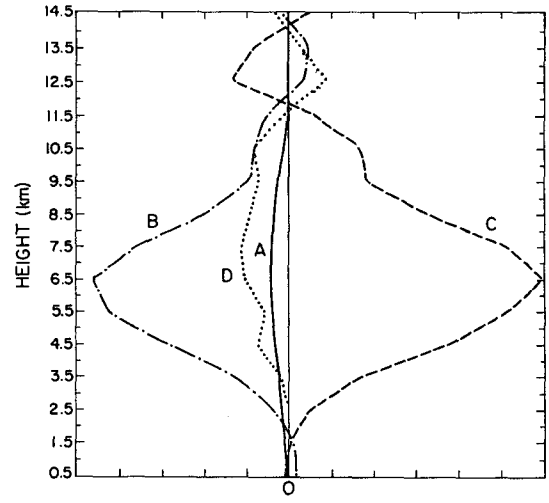

FIG. 6. As in Fig. 5 but for second most unstable mode at wavenumber (−24, 20); $c_r = -14.7$ m s^{-1}, e-folding time = 497 s.

e. *Vertical structure of eigenvectors*

For each wavenumber vector there are *two most unstable* modes with comparable growth rates. Using wind and temperature profiles for the East Atlantic and "Case 1" heating parameters, as in Fig. 4, Figs. 5 and 6 show the vertical structure of the two modes for wavenumber (−24, 20) through a plot of the several terms of the thermodynamic equation. Fig. 5 shows that, for example, the horizontal advection of potential temperature (curve D) is small when compared with the other terms in the lower part of the model. However, above 6.5 km this term almost cancels the adiabatic heating–cooling (curve B). The parameterized cumulus heating (curve A) is quite large, giving rise to a large temperature tendency (curve C) in middle levels.

Figure 6 displays a quite different structure for the second, slightly less unstable mode in that the cumulus heating term (curve A) is relatively minor in comparison with other terms throughout the troposphere. Note that amplitudes at the top of the moist layer (z_{ML}) are rather small. In order to understand this mode, the model was run with the same heating parameters and basic state temperature, but with a vanishing mean flow. Fig. 7 shows that this mode survives in the absence of a mean flow with essentially identical vertical structure. This second mode apparently represents a convective overturning of the atmosphere in which heating serves to initiate the convection.

Examining the several terms of the vertical velocity equation for this case without mean wind (Fig. 8), it is evident that the motion is nonhydrostatic with large vertical velocity accelerations mainly in the lower half

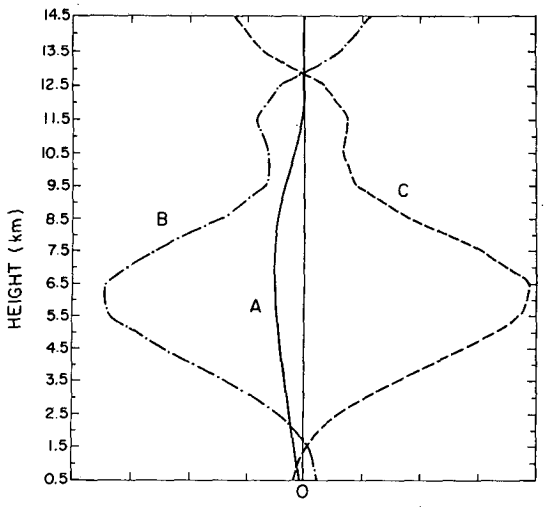

FIG. 7. Same mode as in Fig. 6 but with a motionless basic state; $c_r = -14.5$ m s^{-1}, e-folding time = 490 s.

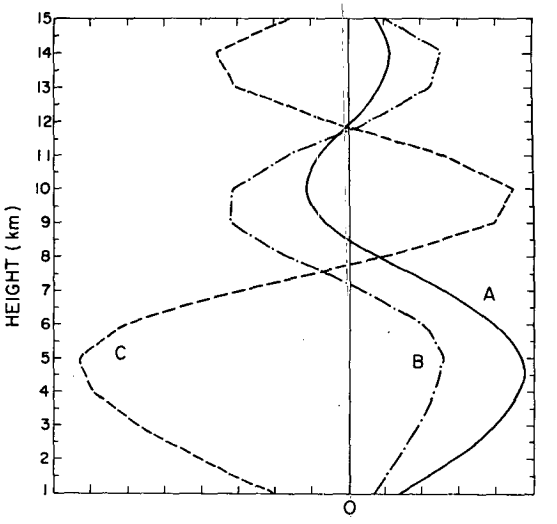

FIG. 8. Vertical structure of terms in the vertical velocity Eq. (14) for the mode of Fig. 7 with a motionless basic state. A (solid line): $\partial w/\partial t$; B (dot-dash line): $\partial/\partial z(p'/\rho_0)$; C (dashed line): $-g(\theta'/\theta_0)$.

of the troposphere. In fact, with wind, the mode of Fig. 5 also has large vertical velocity accelerations. This is understandable since vertical and horizontal scales for that wavenumber are comparable and therefore the hydrostatic approximation should not hold.

6. Sensitivity with respect to basic state

One of the objectives of the present research is to understand the dependence of mesoscale features on large-scale characteristics. We present the sensitivity of the eigenvalues of Eq. (18) to basic state profiles of wind speed, potential temperature and wind direction.

The basic state profiles used are variations about tropical soundings. The winds, for example, are everywhere less than 15 m s^{-1} which is much less than in the environment of midlatitude mesoscale systems.

a. Wind speed

The mean profile over the GATE area, shown in Fig. 2, displays a low-level jet (LLJ) around 600 mb and an upper level jet (ULJ) at 175 mb. For the western Pacific (also shown in Fig. 2) the LLJ is almost nonexistent in the mean obtained by Reed and Recker (1971); the ULJ however, is very pronounced. This section investigates the sensitivity of the eigenvalues of Eq. (18) to the absence or presence of ULJ and LLJ in parallel flow (i.e., without directional wind shear).

The basic state temperature is the one labeled "N^2 = const" in Fig. 3. Fig. 9 shows the zonal component of the E Atlantic wind hodograph of Fig. 2 and also the wind profiles (a) with removal of the LLJ and (b) with removal of ULJ. Case 1 cloud heating parameters are used.

Table 2 summarizes the results obtained. The most striking result is obtained by removing just the LLJ (while keeping the ULJ); the most unstable mode is one which travels to the east (Table 2, case 2) although the second most unstable mode, with growth rate only 10% lower, travels to the west. If, however, the ULJ is removed and only the LLJ is present (Fig. 9b), then the resulting eigenvalues (Table 2, case 3) are almost the same as the ones in Fig. 4 (case 1, Table 1).

In this case, the second most unstable mode (not shown), which travels due east, has growth rates about 30% lower, showing a clear preference for the mode traveling due west.

Observations of squall lines in West Africa (Fortune, 1980) and in the GATE area (Houze, 1977) show ambient winds which clearly have a LLJ. This model test also suggests that the LLJ rather than the ULJ is important to the growth of a westward moving mode, although the phase and group velocity are rather less than those of observed squall lines over land.

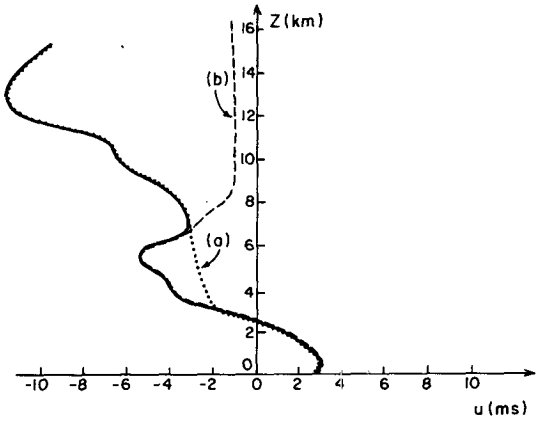

FIG. 9. Zonal component of E Atlantic wind hodograph (solid line) (a) lower level jet, removed (dotted line); (b) upper level jet removed (dashed line).

TABLE 2. Sensitivity of scale selection, phase velocity c_r and group velocity $\mathbf{c}_g$ with regard to basic state wind speed (from Fig. 9) and temperature profile (from (Fig. 3). Case 8 includes directional shear.

Case	Wind	Temperature profile	Scale select (n_x, n_y)	c_r (m s^{-1})	$\mathbf{c}_g$ (m s^{-1})	Direction from (deg)
1	E Atlantic	const N^2	(±14, 0)	±6.6	7.6	90
2	No LLJ	const N^2	(±18, 0)	±8.8	7.6	270
3	No ULJ	const N^2	(±14, 0)	±6.9	5.9	90
4	E Atlantic	const $N^2/2$	(±16, 0)	±4.7	3.3	90
5	E Atlantic	E Atlantic	(±16, 0)	±6.8	4.0	90
6	E Atlantic	W Pacific	(±14, 0)	±4.0	5.0	90
7	E Atlantic	D.248	(±16, 0)	±4.3	3.8	90
8	E Atlantic	const N^2	(−12, 8)	7.4	6.4	130
	Fig. 2		(14, 0)	6.8	6.0	98

b. Potential temperature

The potential temperature profiles in Fig. 3 show that the E Atlantic and W Pacific curves have the same slope from the surface up to 8 km although the E Atlantic curve shows lower temperatures. Above 8 km and below 13 km, the W Pacific curve shows a higher derivative $d\theta_0/dz$, or greater stability. The curve labeled Day 248 shows higher stability below 8 km and about the same slope as the Pacific curve above 8 km.

The eigenvalues of Eq. (18) have been computed for the temperature profiles of Fig. 3 together with the basic state wind of the E Atlantic (Fig. 9). The summarized results may be seen in Table 2. By comparing case 1 and case 4 in Table 2, it may be seen that lowering the static stability, although not producing significant differences in the eigenvalues, diminishes both the phase velocity and the group velocity, while slightly displacing the most unstable mode to a smaller wavelength. Using the other θ profiles in Fig. 3 did not change the results by much, so that we may assume the basic state potential temperature is not as crucial a parameter as the basic state wind field. In what follows, the profile of constant static stability (N^2 in Fig. 3) will be used for simplicity.

c. Directional shear of the wind

This section will show two examples of how crucial the directional shear of the wind can be to the eigenvalues of Eq. (18). Fig. 10 shows the eigenvalues of Eq. (18) using the eastern Atlantic wind profile in Fig. 2. This may be compared with Fig. 4 where the same parameters were used without directional shear. It may be seen that the mode of Fig. 4 has its growth rate intensified by directional shear and its scale displaced so that it travels to the right of the basic state wind. It may be noted also that the basic state winds turn clockwise with height from lower to middle levels. Klemp and Wilhelmson (1978b) have already found intensification of right-moving storms with a clockwise turn of the wind, although their mechanism seems related more to individual cell motion than the mesoscale dynamics.

7. Differences in tropical regimes

In this section, we explore the possibility of whether a linear instability analysis is able to distinguish between different tropical regimes based only on the basic state wind profile.

The profiles chosen are: 1) the ones in Fig. 2 for E Atlantic and W Pacific (Reed and Recker, 1971) mean conditions and 2) wind hodographs for categories 1, 3, 5 and 7 of the Thompson *et al.* (1979) easterly wave (Fig. 11).

For each of the wind hodographs mentioned above, Table 3 shows some features of the two most unstable modes, labeled right moving and left moving mode with respect to the basic state middle to lower level winds. The vector group velocity of these two modes has been plotted over their respective wind hodographs in Figs. 2 and 11 and labeled L for left moving mode and R for right moving mode.

The basic state wind hodographs which turn clockwise with height are: East Atlantic, Category 1, Category 3. *All of these* have a right moving unstable mode with higher growth rate than their left moving counterpart.

The basic state wind hodographs of W Pacific, Category 5 and Category 7, besides having a very weak or almost nonexisting LLJ, turn counterclockwise with height.

For the W Pacific, the left-moving mode is slightly more unstable than the right-moving mode; in Category 7 both left- and right-moving modes have the same growth rates. Category 5 does not show any preferred mode in mesoscale length scales.

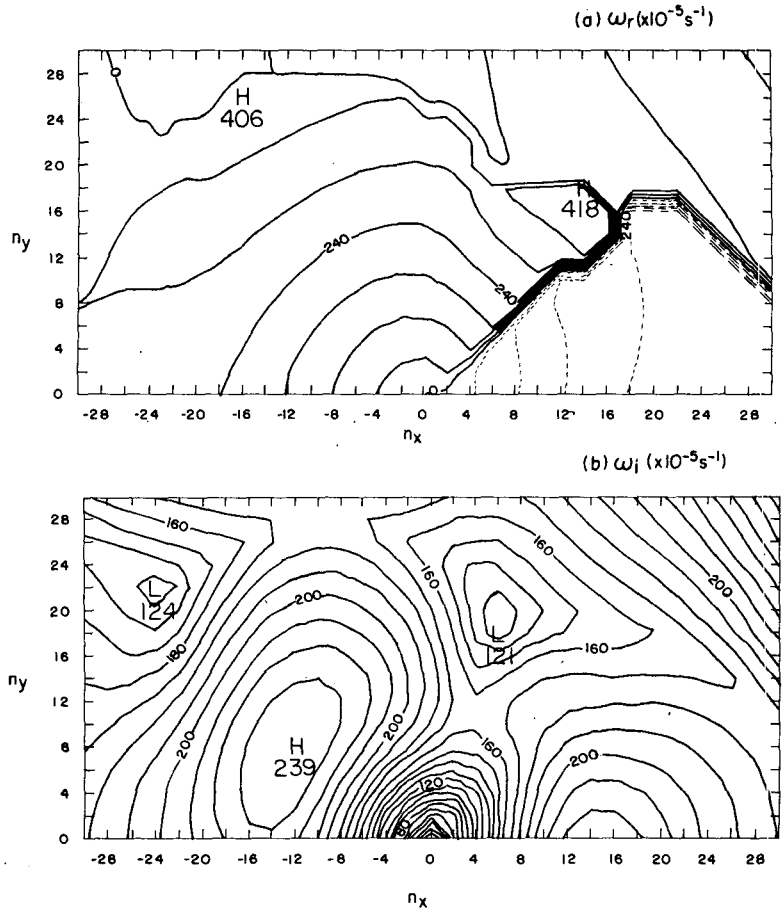

FIG. 10. Eigenvalues of Eq. (18) corresponding to conditions of case 8, Table 2. (a) ω_r, (b) ω_i, units as in Fig. 4.

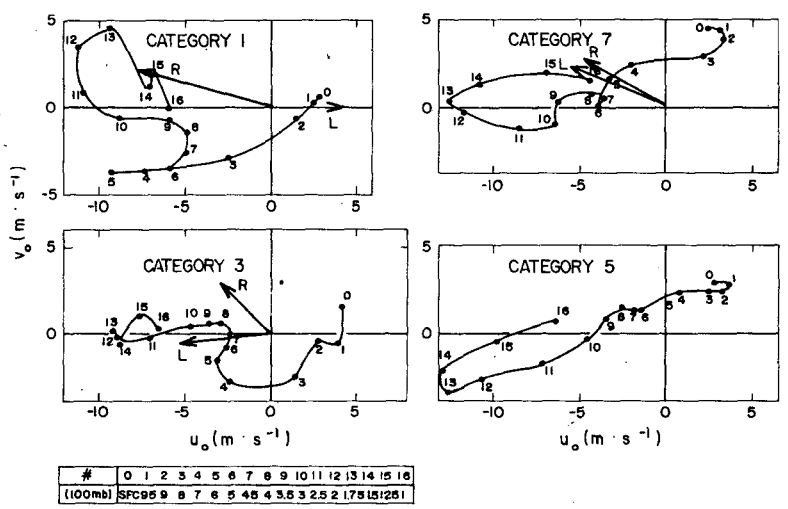

FIG. 11. Wind hodographs for categories 1, 3, 5 and 7 in Thompson *et al.* (1979) composited large-scale easterly wave. L, R denote group velocity vectors associated with left- and right-moving modes.

TABLE 3. Dependence of eigenvalues on basic state winds: differences between tropical regimes and effect of directional shear.

	Right-moving mode					Left-moving mode				
Basic state wind	(n_x, n_y)	L (km)	c_r (m s^{-1})	ω_i (10^{-5} s^{-1})	c_g (m s^{-1}, °)	(n_x, n_y)	L (km)	c_r (m s^{-1})	ω_i (10^{-5} s^{-1})	c_g (m s^{-1}, °)
E Atlantic	(−12, 8)	20.8	7.4	239	6.4, 130	(14, 0)	21.4	−6.8	228	6.0, 98
W Pacific	(−14, 0)	21.4	10.7	173	10.0, 100	(14, 0)	21.4	−10.7	174	9.7, 94
Category 1	(14, 2)	21.2	6.4	227	4.0, 273	(−14, 10)	17.4	7.4	226	8.0, 105
Category 3	(−12, 10)	19.2	5.4	220	4.0, 135	(16, 0)	18.8	−5.5	206	5.3, 84
Category 5	Maximum growth rate for smaller scales —no preferred mode—									
Category 7	(−16, 0)	18.8	6.5	217	5.5, 120	(16, 0)	18.8	−6.5	217	5.5, 114

We thus find, in accordance with Klemp and Wilhelmson (1978b), that there is intensification of the right-moving storm with a clockwise turning of the wind. However, the existence of preferred modes in mesoscale length scales is due primarily to the existence of a LLJ.

8. Conclusions

We have studied the sensitivity of mesoscale models to the parameterization of cumulus heating and the basic state wind and temperature structure using a nonhydrostatic, nonrotating wave-CISK model. The model is a generalization of that of Raymond (1975, 1976) combined with a different cumulus heating parameterization.

We have shown that unstable mesoscale modes exist for wavelengths of ~20 km. In many cases, the most unstable mode has a two-dimensional structure. The structure of these modes (growth rate, group and phase velocity) is sensitive to the cumulus heating parameters, suggesting that appropriate parameterization of cumulus convection remains a crucial problem for wave-CISK models. The wavelength of maximum growth rate (or scale selection) is somewhat less sensitive to the cumulus parameterization.

The range of basic temperature and wind structures used were characteristic of the eastern Atlantic during GATE. The thermal stability does not seem to be a critical parameter, but the unstable modes are clearly sensitive to the wind shear structure. The existence of a low-level jet seems to be important for the selection of a mesoscale unstable mode. The directional shear is also important. Clockwise turning of the wind with height produces a more rapidly growing right moving mode, in agreement with Klemp and Wilhelmson (1978b).

However, there is no close agreement between the model unstable modes and the more complex structure of slow and fast moving convective lines observed during GATE. Most fast moving lines moved westward at 10–15 m s^{-1}, rather faster than the westward moving modes in Fig. 11, whereas the slow-moving lines in GATE moved across the (east–west) wind shear at a few meters per second. Clearly, more work is needed to understand the motion of mesoscale lines.

Acknowledgments. The research presented here has been supported by Grants ATM-8120444 and ATM-8107136 from the National Science Foundation and by Grant N00014-79-C-0793 from the Office of Naval Research.

REFERENCES

Arakawa, A., and W. H. Schubert, 1974: Interaction of a cumulus cloud ensemble with the large-scale environment, Part I. *J. Atmos. Sci.*, **31**, 674–701.

——, and V. R. Lamb, 1977: *Methods in Computational Physics*, Vol. 17, *General Circulation Models of the Atmosphere*, Julius Chang, Ed., Academic Press, 357 pp.

Betts, A. K., 1978: Convection in the tropics. *Meteorology Over the Tropical Oceans*, Roy. Meteor. Soc., 105–132.

Bretherton, F. P., 1969: Momentum transport by gravity waves. *Quart. J. Roy. Meteor. Soc.*, **95**, 213–243.

Brown, J. M., 1979: Mesoscale unsaturated downdrafts driven by rainfall evaporation: A numerical study. *J. Atmos. Sci.*, **36**, 313–338.

Chang, C.-P., 1976: Vertical structure of tropical waves maintained by internally-induced cumulus heating. *J. Atmos. Sci.*, **33**, 729–739.

Charney, J. G., and J. Pedlosky, 1963: On the trapping of unstable planetary waves in the atmosphere. *J. Geophys. Res.*, **68**, 6441–6442.

——, and A. Eliassen, 1964: On the growth of the hurricane depression. *J. Atmos. Sci.*, **21**, 68–75.

Cotton, W. R., 1975: On parameterization of turbulent transport in cumulus clouds. *J. Atmos. Sci.*, **32**, 548–564.

——, and G. J. Tripoli, 1978: Cumulus convection in shear flow—three-dimensional numerical experiments. *J. Atmos. Sci.*, **35**, 1503–1521.

Eliassen, A., and E. Palm, 1960: On the transfer of energy in stationary mountain waves. *Geofis. Publ.*, **22** (No. 3), 1–23.

Emanuel, K. A., 1982: Inertial instability and mesoscale convective systems. Part II: Symmetric CISK in a baroclinic flow. *J. Atmos. Sci.*, **39**, 1080–1097.

Fernandez, W., and A. J. Thorpe, 1979: An evaluation of theories of storm motion using observations of tropical convective systems. *Mon. Wea. Rev.*, **107**, 1306–1319.

Fortune, M., 1980: Properties of African squall lines inferred from time-lapse satellite imagery. *Mon. Wea. Rev.*, **108**, 153–168.

Fritsch, J. M., 1978: Parameterization of midlatitude organized convection. Ph.D. thesis, Colorado State University, 143 pp.

Gray, W. M., 1977: Tropospheric mean state and variability. *Report of the U.S. GATE Central Program Workshop*, NCAR, Boulder, CO, 199–213.

Hayashi, Y., 1970: A theory of large-scale equatorial waves generated by condensation heat and accelerating the zonal wind. *J. Meteor. Soc. Japan,* **48,** 140–160.

Houze, R. A., 1973: A climatological study of vertical transports by cumulus-scale convection. *J. Atmos. Sci.,* **30,** 1112–1123.

——, 1977: Structure and dynamics of a tropical squall-line system. *Mon. Wea. Rev.,* **105,** 1540–1567.

——, and C. P. Chang, 1977: Radar characteristics of tropical convection observed during GATE: Mean properties and trends over the summer season. *Mon. Wea. Rev.,* **105,** 964–980.

Johnson, R. H., 1978: Cumulus transports in a tropical wave composite for Phase III of GATE. *J. Atmos. Sci.,* **35,** 484–494.

Klemp, J. B., and R. B. Wilhelmson, 1978a: The simulation of three-dimensional convective storm dynamics. *J. Atmos. Sci.,* **35,** 1070–1096.

——, and ——, 1978b: Simulation of right-and-left moving storms produced through storm splitting. *J. Atmos. Sci.,* **35,** 1097–1110.

Koss, W. J., 1976: Linear stability of CISK-induced disturbances: Fourier component eigenvalue analysis. *J. Atmos. Sci.,* **33,** 1195–1222.

Kreitzberg, C. W., and D. J. Perkey, 1976: Release of potential instability: Part I. A sequential plume model within a hydrostatic primitive equation model. *J. Atmos. Sci.,* **33,** 456–475.

——, and ——, 1977: Release of potential instability: Part II. The mechanism of convective mesoscale interaction. *J. Atmos. Sci.,* **34,** 1569–1595.

Lindzen, R. S., 1974: Wave-CISK in the tropics. *J. Atmos. Sci.,* **31,** 156–179.

Moncrieff, M. W., and J. S. A. Green, 1972: The propagation and transfer properties of steady convective overturning in shear. *Quart. J. Roy. Meteor. Soc.,* **98,** 336–352.

——, and M. J. Miller, 1976: The dynamics and simulation of tropical cumulonimbus and squall lines. *Quart. J. Roy. Meteor. Soc.,* **102,** 373–394.

Nitta, T., 1977: Response of cumulus updraft and downdraft to GATE A/B-scale motion system. *J. Atmos. Sci.,* **34,** 1163–1186.

Ooyama, K., 1963: A dynamical model for the study of tropical cyclone development. *Geofis. Int.,* **4,** 187–198.

——, 1969: Numerical simulation of the life cycle of tropical cyclones. *J. Atmos. Sci.,* **26,** 3–40.

Pedlosky, J., 1964: An initial value problem in the theory of barotropic instability. *Tellus,* **16,** 12–17.

Raymond, D. J., 1975: A model for predicting the movement of continuously propagating convective storms. *J. Atmos. Sci.,* **32,** 1308–1317.

——, 1976: Wave-CISK and convective mesosystems. *J. Atmos. Sci.,* **33,** 2392–2398.

Reed, R. J., and E. E. Recker, 1971: Structure and properties of synoptic scale wave disturbances in the equatorial western Pacific. *J. Atmos. Sci.,* **28,** 1117–1133.

Schneider, E. K., and R. S. Lindzen, 1976: A discussion of the parameterization of momentum exchange by cumulus convection. *J. Geophys. Res.,* **81,** 3158–3160.

Silva Dias, M. F., 1979: Linear spectral model of tropical mesoscale systems. Atmos. Sci. Pap. No. 311, Colorado State University, Ft. Collins, 213 pp.

Stevens, D. E., and R. S. Lindzen, 1978: Tropical wave-CISK with a moisture budget and cumulus friction. *J. Atmos. Sci.,* **35,** 940–961.

Sun, W. Y., 1978: Stability analysis of deep cloud streets. *J. Atmos. Sci.,* **35,** 466–483.

Thompson, R. M., Jr., S. W. Payne, E. E. Recker and R. J. Reed, 1979: Structure and properties of synoptic-scale wave disturbances in the intertropical convergence zone of the eastern Atlantic. *J. Atmos. Sci.,* **36,** 53–72.

Williams, K. T., and W. M. Gray, 1973: Statistical analysis of satellite observed trade wind cloud clusters in the western North Pacific. *Tellus,* **25,** 313–336.

Yamasaki, M., 1969: Large-scale disturbances in the conditionally unstable atmosphere in low latitudes. *Pap. Meteor. Geophys.,* **20,** 289–336.

Yanai, M., W. Esbensen and J. H. Chu, 1973: Determination of bulk properrties of tropical cloud clusters from large-scale heat and moisture budgets. *J. Atmos. Sci.,* **30,** 611–627.